NANOSTRUCTURED PHOTOCATALYTIC TITANIA THIN-FILMS: THE EFFECT OF FILM MORPHOLOGY ON PHOTOELECTROCHEMICAL PROPERTIES

Rafael McDonald and Pratim Biswas
Washington University in St. Louis, Department of Environmental Engineering Science,
One Brookings Drive, Campus Box 1180, St. Louis, MO 63130

Extended Abstract

Hydrogen has been touted as the fuel of the future[1]. Since hydrogen is an element, it contains no carbon, and its use as a fuel, either in combustion or in a fuel-cell, leads to only water as a byproduct. Current techniques for hydrogen generation, however, rely upon steam reforming of hydrocarbons. This is problematic because the 1) hydrocarbons are produced on geologic timescales, which are much slower than current consumption requirements, and 2) the byproducts are carbonaceous greenhouse gasses. The photosplitting of water using solar energy is a potentially *clean* and *renewable* source of hydrogen fuel that is environmentally benign and easily distributed. Light impacting titanium dioxide electrodes immersed in water causes the water to split into oxygen and hydrogen[2]. However, pure bulk TiO_2 requires UV-light (which is less than 5% of incident solar radiation) for excitation.

Recent reports in the literature have indicated that some materials such as $In_{1-x}Ni_xTaO_4$[3] and WO_3 doped titanium dioxides[4] are capable of harvesting *visible* sunlight to produce hydrogen and oxygen. The synthesis of such materials remains a challenge, since these compounds are produced by multi-step processes which are often difficult to replicate and even more difficult to scale-up. Advances in gas phase nanoparticle synthesis techniques offer hope that such materials could be synthesized that achieve breakthroughs in photocatalysis.

It has been shown that for titanium dioxide semiconducting photocatalysts[5], particles involved in splitting water have optimal conversion efficiencies in the nanoparticle sizes, as quantum effects become more important. At such small sizes though, however, detrimental recombination of electrons and hole pairs occur more frequently on the surface of the particles. As such, there is an as-of-yet undetermined optimal particle size for water splitting, where quantum effects gains are balanced with surface recombination losses.

Doping of titanium dioxide is a common way to shift the absorption spectrum into the visible regime. It has been shown for other photocatalytic reactions that there is an optimal dopant concentration[6], and furthermore, that this concentration is dependent upon the particle size[7]. The literature also lacks information indicating how other aspects of the morphology (packing density, surface roughness, fractal dimensions, etc.) of the particles may affect efficiency. Models currently exist that predict the effect of gas-phase deposition conditions on thin film characteristics[8;9], but some of these conditions have yet to be experimentally verified. Lastly, the effect of the film morphology on system performance is not well understood.

In this work, we demonstrate the effect that different process conditions have on the physical (particle size, morphology, crystal structure) and electrical characteristics of the thin film. Titania films were created via Dip-Coating (DC), Precursor-Vapor Deposition (PVD) and

Flame Aerosol Deposition (FAD) onto stainless steel substrates. Process conditions were varied, and the effect on the morphology of the film was explored by various methods. SEM micrographs were analyzed for primary particle size, as well as gross morphology. AFM images were analyzed for surface fractal dimension (D_a) via the Shifting Differential Box Counting (SDBC) method.[10;11] The films were examined as deposited via XRD for crystal structure and crystallite size, and relative anatase/rutile fractions were calculated via the method of Spurr and Meyers.[12]

Dip coating led to the simplest films composed of unsintered primary particles (**Figure 1**). They had the lowest roughness (36nm) and the lowest fractal dimension (2.59). Large cracks formed in the film upon drying. As the suspension used for the DC method was made of Degussa P25, the crystallinity (77.3% Anatase) and primary particle size (d_{pg}=30.2nm, σ_g=1.26) were predetermined.

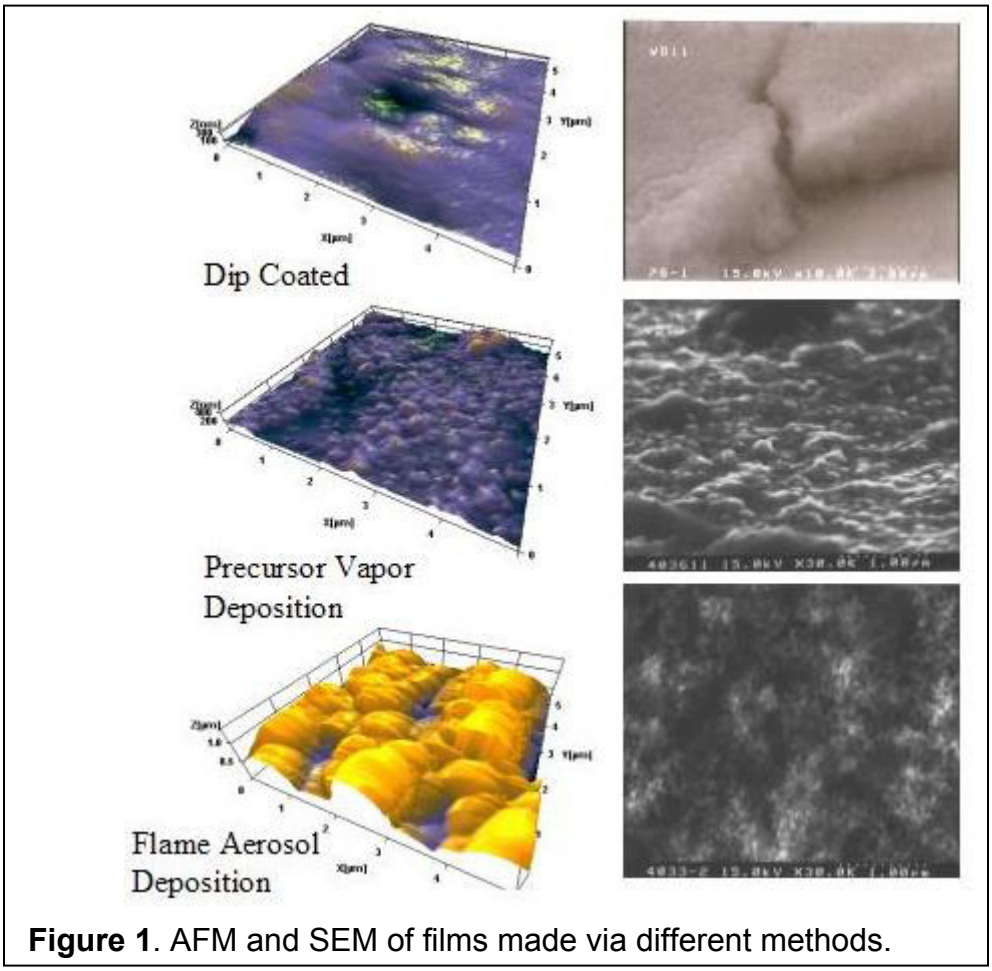

Figure 1. AFM and SEM of films made via different methods.

Precursor vapor deposition led to unevenly deposited films with low roughness (40nm) and a slightly more disordered surface structure (D_a=2.67). High heat was used in this method to decompose the precursor on the slide, but also had the effect of sintering some of the particles that had already been deposited. As such, the primary particle size was considerably larger (d_{pg}=80.34, σ_g=1.21). Despite the high temperatures involved in this method, rutilization did not occur to a great extent (89.3% anatase).

Films generated via Flame Aerosol Deposition were highly porous dendritic structures very similar to those described in Kulkarni and Biswas.[8] Primary particles showed very little sintering. Analysis of these films showed a low anatase fraction (70%), but a great enhancement in particle size (d_{pg}=16.3nm, σ_g=1.21) and surface structure (roughness of 191nm and D_a of 2.75). As such, further films were generated with this method at different process conditions.

FAD deposited films were generated with various configurations and flow rates, resulting in quite different morphologies. The use of a two-port FAD reactor with low feed rates (FAD_2-low) led to highly elongated aggregates (**Figure 2**) composed of primary particles with d_{pg} of 43nm (σ_g=1.50). These structures were highly diluted on the substrate surface, and

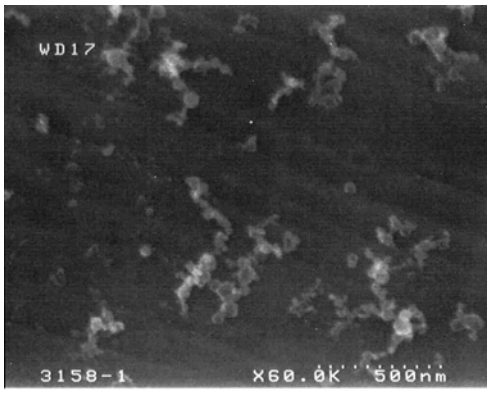

Figure 2 – Linear growth generated in FAD_2 system with low feedrates and low dilution.

deposition occurred mostly along the plane of the surface (xy plane). The particles most resembled diffusion-limited cluster-cluster growth[13]. Higher feed rates in the same flame configuration (FAD_2-high) with high dilution rates led to thicker films (**Figure 3**), with aggregates composed of larger primary particles

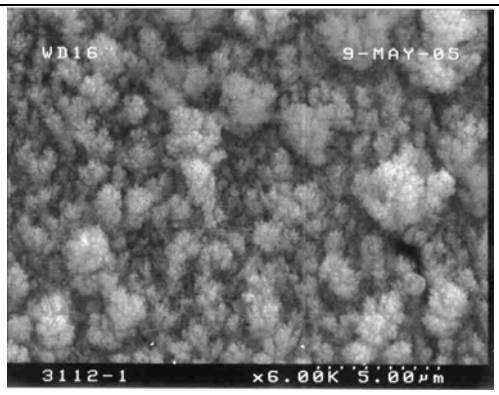

Figure 3 – Columnar growth generated in FAD_2 system under high feedrates and high dilution

(d_{pg}=73nm, σ_g=1.31). Particle density was high, and the primary direction of growth perpendicular to the surface (z direction). The resulting aggregates had the characteristic morphology of reaction-limited particle-cluster growth.[13]

Three-port Flame Aerosol Deposition (FAD_3) also led to RLPC-like aggregates, but with much smaller particle sizes. The particle size was found to be a function of both residence time (**Figure 3**) and precursor feedrate in the flame (**Figure 4**). By controlling these two parameters, the primary particle size was fairly easily controlled. Film thickness grew

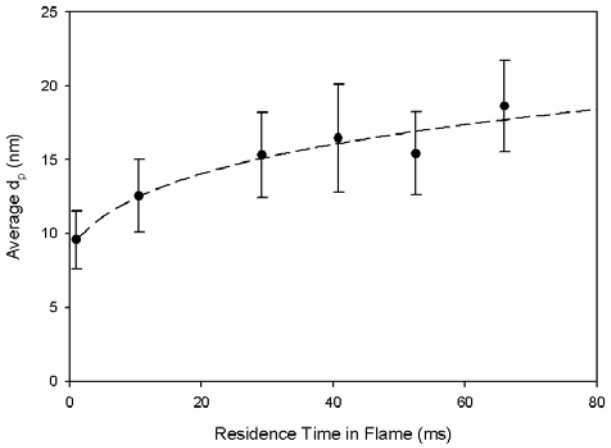

Figure 3. Effect of residence time (burner to substrate) on primary particle size in the Flame Aerosol Deposition system.

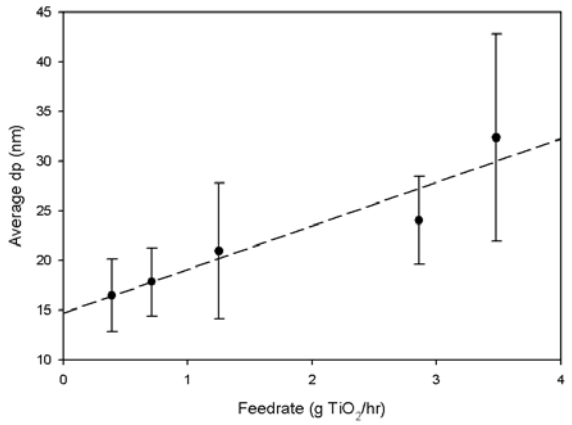

Figure 4. Effect of precursor feedrate on primary particle size in the Flame Aerosol Deposition system.

logarithmically, in contrast to the theoretical work of Kulkarni and Biswas who predicted a decrease in surface coverage with increasing film thickness.[8] The model employed in that study assumed a constant thermophoretic force. As the film grows, however, the temperature at the film-gas interface increase, as the deposited particles are not perfect heat conductors. This effectively decreases the thermophoretic force and, subsequently, the film growth rate. Maedler et al. (2005) accounted for this decrease in thermophoretic force, and predict the logarithmic shape that was obtained in this study.[9]

As shown previously, increasing the feedrate led to an increase in primary particle size, but it also led to a decrease in roughness and fractal dimension. The pertinent details are given in **Table 1**.

Table 1: Size and surface structure of films generated under different conditions

Deposition Method	Feedrate (g TiO_2/hr)	d_{pg} (nm)	Roughness (nm)	D_a (-)
PVD	0.39	80.3	40	2.67
FAD	0.39	16.3	191	2.75
FAD	1.25	19.7	53	2.67
FAD	3.48	33.9	29	2.60

Photocurrents (current under 365nm illumination minus current in the dark) were measured under short-circuit conditions for different films. **Figure 5** shows the photocurrents for the films tested. The response of the FAD film (16.3nm primary particles) is a classic

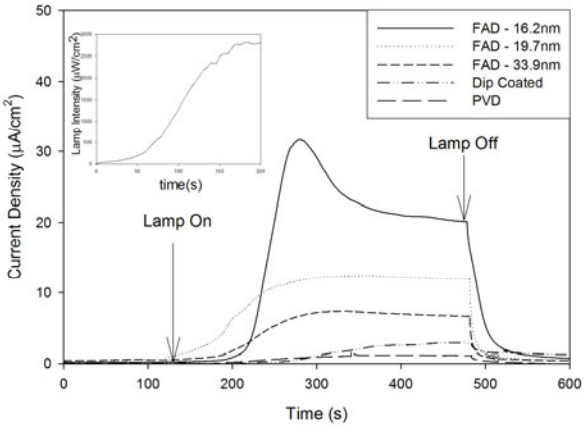

Figure 5. Photocurrent responses for films generated under different conditions. Note that the film with the highest steady state current is the only one that displays the typical anodic spike classically seen in semiconductor responses.

photoresponse of a semiconductor. At a fixed potential, the electrode has a steady dark current. When the electrode is illuminated, electron-hole pairs in the space-charge region separate, leading to the observed anodic spike. The response is not immediate; however, as the lamp requires some time to reach maximum output (see inset). Once the maximum current is reached, the photocurrent then decays to a steady-state value, indicating that a portion of the holes that reach the surface are either recombining with electrons in the conduction band or accumulating at the surface, rather than reacting with electrons from the electrolyte[14;15]. The process is mass-transfer limited. When the illumination stops, the current quickly decays back to the dark current values.

The other four films (DC, PVD, and FAD_3 films with primary particles of 19.7 and 33.9nm) show a similar trend, but with important distinctions. None of these films show the same anodic spike as seen in the 16.3nm FAD_3 film. This indicates that all of the holes reaching the surface are reacting with the electrolyte. Mass transfer of electrolyte to the surface is not the limiting factor. Instead, either electron-hole production or the migration of electrons and holes to the surface is the limiting factor. Given that the size of the particles is larger in all of these cases, transport of the electrons and holes to the surface is the most likely explanation.

The second important difference between the films is the actual steady-state photocurrents. All of the FAD films displayed photocurrents much higher than those produced by DC and PVD films. Between the FAD films, one sees that the smaller the primary particle, the larger the photocurrent. In this system with these primary particle sizes, the decrease in photoactivity due to quantum effects (seen in some systems[5] but not in others[16]) has not become an important factor. As the particle size decreases, the time required for electron-hole transfer to the surface decreases. This decreases the likelihood of electron-hole recombination, and therefore increases efficiency.

Open cell potentials were also measured vs. time. As **Figure 6** shows, even the best performing film (FAD_3 with primary particles of 16.3nm) only achieved 600mV, which is slightly

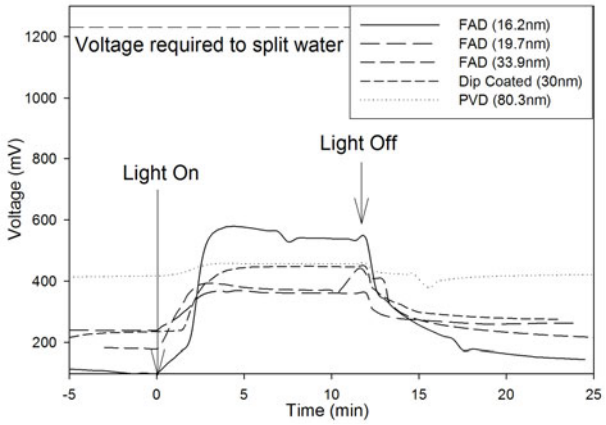

Figure 6. Photovoltage responses for films generated under different conditions. Even the best response fails to generate the 1.23V required to split water.

less than half of the required 1.23V required for the photosplitting of water. Again, films generated via FAD_3 performed the best, with an increase in performance with decreasing primary particle size.

Unlike the work of Almquist and Biswas[5] who studied the decomposition of phenol, a maximum efficiency was not found. Instead, the efficiency was found to increase with decreasing primary particle size. However, in other systems, the same maximum efficiency was found to occur at sizes even smaller than those studied in this system.[16] As such, efforts will continue to decrease the primary particle size, to ascertain at which point quantum inefficiencies begin to compete with increased surface area effects. In addition, further efforts will be made to decouple the processes that change primary particle size and surface characteristics, so to ascertain the relative importance of each parameter.

Bibliography

1. US Department of Energy. *Hydrogen Posture Plan: An Integrated Research, Development, and Demonstration Plan*; US Department of Energy, Office of Energy Efficiency and Renewable Energy: Washington, D.C., 2004.
2. Honda, K.; Fujishima, A. Electrochemical Photolysis of Water at a Semiconductor Electrode. *Nature*, **1972**, *238*, 37-38.
3. Zou, Z.; Ye, J.; Sakayama, K.; Arakawa, H. Direct Splitting of Water Under Visible Light Irradiation With an Oxide Semiconductor Photocatalyst. *Nature*, **2001**, *414*, 625-627.
4. Ohno, T.; Tanigawa, F.; Fujihara, K.; Izumi, S.; Matsumura, M. Photocatalytic Oxidation of Water on TiO2-Coated WO3 Particles by Visible Light Using Iron(III) Ions as Electron Acceptor. *Journal of Photochemistry and Photobiology A: Chemistry*, **1998**, *118*, 41-44.
5. Almquist, C. B.; Biswas, P. Role of Synthesis Method and Particle Size of Nanostructured TiO2 on Its Photoactivity. *Journal of Catalysis*, **2002**, *212*, 145-156.
6. Kaneko, M.; Okura, I. *Photocatalysis: Science and Technology*; Springer: New York, **2002**.
7. Zhang, Z.; Wang, C.-C.; Zakaria, R.; Ying, J. Role of Particle Size in Nanocrystaline TiO2 Based Photocatalysts. *Journal of Physical Chemistry B*, **1998**, *102*, 10871-10878.
8. Kulkarni, P.; Biswas, P. Morphology of Nanostructured Films for Environmental Applications: Simulations of Simultaneous Sintering and Growth. *Journal of Nanoparticle Research*, **2003**, *5*, 259-268.
9. Maedler, L.; Roessler, A.; Pratsinis, S. E.; Sahm, T.; Gurlo, A.; Barsan, N.; Weimar, U. Direct Formation of Highly Porous Gas-Sensing Films by in-situ Thermophoretic Deposition of Flame-Made Pt/SnO2 Nanoparticles. *Sensors and Actuators B: Chemical*, **2005**, *Article in Press*,
10. Chen, W. S.; Yuan, S.-Y.; Hsieh, C.-M. Two Algorithms to Estimate Fractal Dimension of Gray-Level Images. *Optical Engineering*, **2003**, *42*, 2452-2464.
11. Henden, P. C.; Bache-Wiig, J. MapFractalCount; Haugesund, Norway, 2004. http://www.pvv.org/~perchrh/imagej/.
12. Spurr, R.; Myers, H. Quantitative Analysis of Anatase-Rutile Mixtures with an X-Ray Diffractometer. *Analytical Chemistry*, **1957**, *29*, 760-762.
13. Friedlander, S. K. *Smoke Dust and Haze: Fundamentals of Aerosol Dynamics*; Oxford University Press: New York, NY, **2000**.
14. Byrne, J. A.; Eggins, B. R. Photoelectrochemistry of Oxalate on Particulate TiO2 Electrodes. *Journal of Electroanalytical Chemistry*, **1998**, *457*, 61-72.
15. Byrne, J. A.; Eggins, B. R.; Brown, N. M. D.; McKinney, B.; Rouse, M. Immobilisation of TiO2 Powder for the Treatment of Polluted Water. *Applied Catalysis B: Environmental*, **1998**, *17*, 25-36.
16. Maira, A. J.; Yeung, K. L.; Lee, C. L.; Yue, P. L.; Chan, C. K. Size Effects on Gas-Phase Photo-Oxidation of Trichloroethylene Using Nanometer -Sized TiO2 Catalysts. *Journal of Catalysis*, **2000**, *192*, 185-196.